

Image Deblurring via Extreme Channels Prior

Yanyang Yan^{1,2}, Wenqi Ren^{1,3}, Yuanfang Guo¹, Rui Wang¹, and Xiaochun Cao^{1,2,*}

¹State Key Laboratory of Information Security, IIE, Chinese Academy of Sciences

²School of Cyber Security, University of Chinese Academy of Sciences

³School of Computer Science and Technology, Tianjin University

Abstract

Camera motion introduces motion blur, affecting many computer vision tasks. Dark Channel Prior (DCP) helps the blind deblurring on scenes including natural, face, text, and low-illumination images. However, it has limitations and is less likely to support the kernel estimation while bright pixels dominate the input image. We observe that the bright pixels in the clear images are not likely to be bright after the blur process. Based on this observation, we first illustrate this phenomenon mathematically and define it as the Bright Channel Prior (BCP). Then, we propose a technique for deblurring such images which elevates the performance of existing motion deblurring algorithms. The proposed method takes advantage of both Bright and Dark Channel Prior. This joint prior is named as extreme channels prior and is crucial for achieving efficient restorations by leveraging both the bright and dark information. Extensive experimental results demonstrate that the proposed method is more robust and performs favorably against the state-of-the-art image deblurring methods on both synthesized and natural images.

1. Introduction

Blind image deblurring attracts considerable research attention in computer vision community. With the assumption that the blur is uniform and spatially invariant, the mathematical formulation of the blurry image can be modeled as,

$$b = l \otimes k + n, \quad (1)$$

where b , l , k and n are blurry observation, latent image, blur kernel and noise, respectively. Also, \otimes denotes the convolution operator. Blind image deblurring aims to recover the blur kernel k and the corresponding latent image l from a blurry input image b , which is a highly ill-posed problem, because many different pairs l and k can give rise to the

same b . Therefore, additional information or constraints are required to solve this problem.

In general, most existing methods take advantage of the prior knowledge of the statistics of natural images. Such as heavy-tailed gradient distributions [5, 13], normalized sparsity prior [12], L0-regularized gradient [25], patch recurrence prior [15], and a combination of the intensity and gradient prior [16]. Recently, Pan *et al.* [17] present an valid blind image deblurring method based on the dark channel prior [6]. This algorithm enforces the sparsity of the dark channel of latent images for kernel estimation and generates better results compared to other approaches. However, larger degrees of bright pixels or noise can significantly affect the performances of this algorithm since the dark channel prior do not hold under this circumstances.

In this paper, we propose a blind image deblurring algorithm based on a novel natural image prior named Bright Channel Prior (BCP). Inspired by the work in [17], we observe that the bright channel pixels (pixels with the largest channel value within the local patch) are no longer bright after the blurring process. We prove this empirical observation mathematically and exploit this property to recover the intermediate image for kernel estimation. Therefore, we propose to maximize the bright channel of the clear image by exploiting an L_0 -regularization term of inverse BCP. Optimizing the L_0 -regularized term is challenging. In the proposed algorithm, we solve the non-convex L_0 -minimization problem by employing the half-quadratic splitting method [24].

The core contributions are summarized as follows.

- We propose a novel natural image prior named Extreme Channels Prior (ECP) by taking the advantages of both DCP and BCP.
- We prove that the values of bright channel pixels decrease after blurring process and validate our theories by comparing the intensities of bright channel pixels of 5,000 natural images and the corresponding blurry ones.
- We exploit the bright channel prior to help kernel esti-

*Corresponding author.

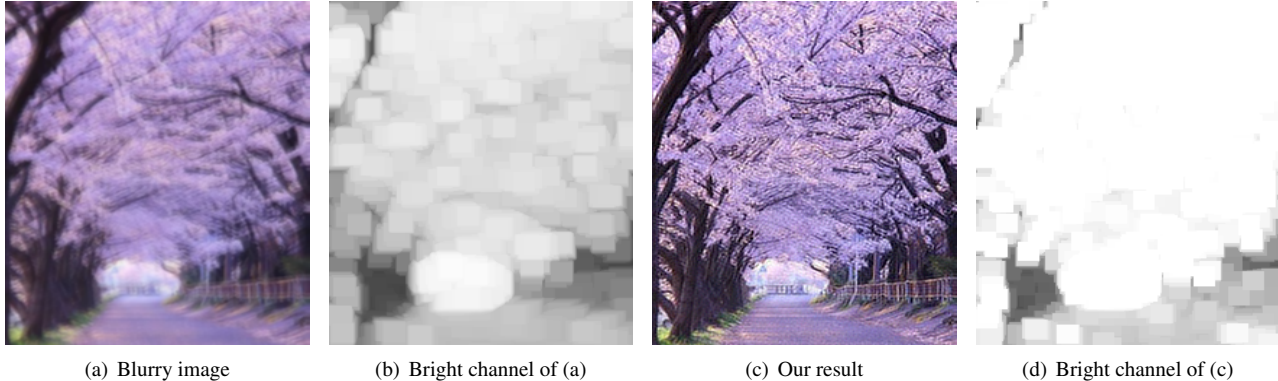


Figure 1. Our deblurring result of a blurry image. The intensities of bright channel pixels decrease after the blurring process. Maximizing the bright channel helps image recovering.

mation as an L0-regularization term to change the sparsity and develop an efficient optimization scheme.

2. Related Work

In recent years, significant progress has been witnessed in blind image deblurring. Extensive methods take advantage of sharp edges to estimate blur kernel [10, 19, 21]. Joshi *et al.* [10] propose to utilize sub-pixel differences precision to detect edges for kernel estimation. Cho and Lee [19] present a multi-scale framework using simple image filters to restore sharp edges from blurry pictures. While these approaches work well for small blur kernels, they have difficulty dealing with large scale kernels. In [21], Sun *et al.* derive a novel patch-based strategy to improve Cho’s method [19] for the same objective. However, this algorithm is computationally expensive and not practical due to querying a large dataset process.

To estimate blur kernels from blurry images, other existing approaches utilize statistical priors[4, 20, 14, 12, 25, 16] or additional information [8, 3, 9] to solve the ill-posed problem. Shan *et al.* [20] adopt a sparse image prior and introduce a unified probabilistic model to fit the gradient distribution of natural images. Levin *et al.* [14] model the latent images using a hyper-Laplacian prior and derive a simple approximation method to optimize the maximum a posterior (MAP) framework. Various natural image priors are used in deblurring that favor clear images rather than blurry ones. In [12], a minimization scheme is proposed by utilizing L_1/L_2 regularizer for edge selection. While these techniques help kernel estimation, they may lose some details in the early stage during deblurring. Hu *et al.* [8] use the light streaks to help low-light images deblurring.

Recently, L_0 sparse representation is developed and incorporated into regularization in [25] for deblurring. Pan *et al.* [16] promote this approach by applying L_0 -regularized prior on both intensity and gradient for specific text image

deblurring. In [17], a genetic approach is proposed by considering how dark channel pixels vary during the blur process. The dark channel prior was first introduced by He *et al.* [6] based on the observation that in most of the natural scene patches, at least one of the color channels possesses some pixels with very close to zero intensities. Pan *et al.* [17] modify the prior that the dark channel of natural images is sparse instead of zero and enforce the sparsity for kernel estimation. While this work have robust performance on various benchmark datasets, the dark channel prior may not help intermediate latent image estimation if no dark pixels exist in the image.

3. Bright Channel Prior

In this section, we first present a novel statistical prior, *i.e.*, BCP, and then prove this prior mathematically. This prior is based on the observation that in most of the natural scene patches, at least one of the color channels possesses pixels with very large intensity. To formally describe this observation, we define the bright channel of an image I as

$$B(I)(x) = \max_{y \in \Omega(x)} \left(\max_{c \in (r, g, b)} I^c(y) \right), \quad (2)$$

where x is the pixel location, I^c is a color channel of I and $\Omega(x)$ denotes a local patch centered at x . As we can observe from Eq. (2), a bright channel is the outcome of two maximum operators: $\max_{c \in (r, g, b)}$ and $\max_{y \in \Omega(x)}$. Note that if I is a gray-scale image, only the latter operator performs. By utilizing this concept, we conclude that the intensity of $B(I)$ should be high and close to one, except for the situation which lacks the light or the shadow dominates. We name our observation as BCP.

The high intensities in the bright channel are mainly due to three factors: 1) light. *e.g.*, sunlight, light from other existing light sources, and the sky regions in the daytime which are illuminated by the sun; 2) white or bright objects

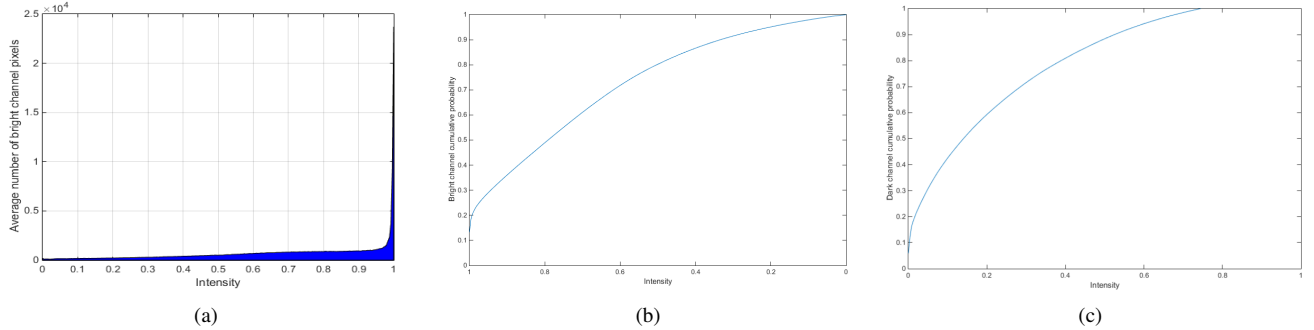


Figure 2. Statistics of the bright and dark channels. (a) Histogram of the intensity of the pixels in all of the 5,000 bright channels. (b)-(c) Cumulative distribution of bright and dark channels, respectively.

or surfaces. *e.g.*, white walls, floors, etc. 3) bright-colored objects or surfaces, *e.g.*, objects with high reflectance in at least one of color channels, such as green leaf, yellow flower and blue water, will also lead to high intensities in their bright channel. We further validate our observation with the statistics of the bright channels by randomly selecting 5000 images from the PASCAL 2012 dataset [1] without any manually pre-processing. Figure 2(a) shows the histogram of the average number of bright channel pixels. As can be observed, a large portion of the pixels in the bright channels possess very large values, which strongly supports our proposed prior. Figure 2(b) is the cumulative distribution of the bright channels and Figure 2(c) is the corresponding cumulative distribution of the dark channels. Note that for the convenience of comparison, we reverse the horizontal x-axis of Figure 2(b). We can conclude that our BCP is comparable to the classical DCP.

To utilize our BCP during deblurring, we analyze how bright channels vary after the blurring process. Note that the blur model in Eq. (1) resembles the convolution process except for the noise. For comparison, we consider blurring with the assumption that the noise is small enough to be neglected. Formally, we have

$$b(x) = \sum_{z \in \Phi(x)} l(x - z + [\frac{p}{2}])k(z), \quad (3)$$

where $\Phi(x)$ denotes the blur patch centered at pixel x with size p , which is identical to the size of blur kernel k . In addition, $[.]$ is the rounding process. According to the property of blurring, we have $k(z) \geq 0$ and $\sum_{z \in \Phi(x)} k(z) = 1$. Let p equal to the patch size of $\Omega(x)$ in Eq. (2), we can obtain

$$\begin{aligned} b(x) &= \sum_{z \in \Phi(x)} l(x - z + [\frac{p}{2}])k(z) \\ &\leq \sum_{z \in \Phi(x)} \max_{y \in \Omega(x)} l(y)k(z) \\ &= \max_{y \in \Omega(x)} l(y) \sum_{z \in \Phi(x)} k(z) \\ &= \max_{y \in \Omega(x)} l(y). \end{aligned} \quad (4)$$

Eq. (4) shows that the intensity at pixel x after the blur operation is not more than the maximum intensity of the pixels in the original image patch centered at x . Particularly, if x is the brightest pixel in its local patch, Eq. (4) is equal to $b(x) \leq l(x)$. To further apply this proposition to the definition of bright channel, it satisfies,

$$\begin{aligned} B(b)(x) &= \max_{y \in \Omega(x)} (\max_{c \in (r, g, b)} b^c(y)) \\ &= \max_{y \in \Omega(x)} b(y) \\ &= \max_{y \in \Omega(x)} \sum_{z \in \Phi(y)} l(y - z + [\frac{p}{2}])k(z) \\ &\leq \sum_{z \in \Phi(y)} \max_{y \in \Omega(x)} l(y - z + [\frac{p}{2}])k(z) \\ &\leq \sum_{z \in \Phi(y)} \max_{y^l \in \Omega^l(x)} l(y^l)k(z) \\ &= \max_{y^l \in \Omega^l(x)} l(y^l) \\ &= B(l)(x). \end{aligned} \quad (5)$$

Let S_Ω and S_{Ω^l} denote the size of the bright channel patch $\Omega(x)$ and $\Omega^l(x)$, respectively. Then we can obtain $S_{\Omega^l} = S_\Omega + p$. To preserve this property, we adopt large bright channel patch. Eq. (5) demonstrates that the bright channel of a blurry image has lower pixels intensities than the corresponding one of clear image. Therefore, a property which is helpful to the kernel estimation is introduced that the blur process reduces pixels values which are equal to one in the latent image. Formally, we have

$$\|1 - B(b)(x)\|_0 \geq \|1 - B(l)(x)\|_0. \quad (6)$$

Note that the intensity of the brightest pixels is 1 and the equality sign can be satisfied if and only if the intensities of all the pixels in $\Phi(x)$ are lower than 1 or identical to each other. In addition, this property holds regardless of the size of bright channels patch. We also validate this statistics on the PASCAL 2012 dataset. Figure 3 shows that the bright channels of the latent images possess more values

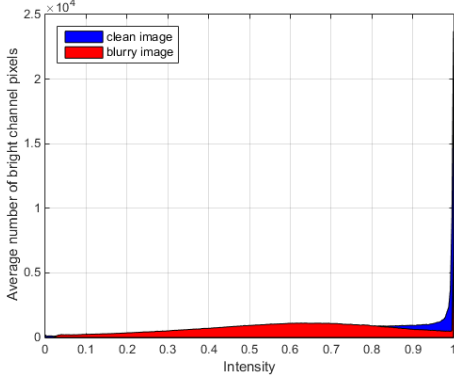


Figure 3. Intensity histograms of bright channels of both clear and blurred images in 5,000 natural images.

which are close to one than those of corresponding blurry images. This statistical property gives very strong support to our analysis above. Motivated by Eq. (6), in this paper, we enforce this L_0 -norm sparsity as a novel regularization term for image deblurring.

4. Proposed Algorithm

In this section, we present a blind image deblurring model and develop an efficient optimization algorithm for kernel estimation. We formulate the deblurring problem within the maximum a posteriori (MAP) framework as [25],

$$\{\hat{l}, \hat{k}\} = \arg \min_{l, k} \ell(l \otimes k, b) + \gamma p(k) + \lambda p(l), \quad (7)$$

where $p(k)$ and $p(l)$ are the priors of the blur kernel and the latent image, respectively.

4.1. Proposed ECP

Motivated by our proposed BCP and the corresponding analysis in Section 3, we present a novel L_0 -regularization of the inverse BCP based image prior as

$$p(l) = \|1 - B(l)\|_0. \quad (8)$$

Then we propose a novel ECP for image deblurring by taking the advantage of both the proposed BCP and the familiar DCP.

$$p(l) = \|1 - B(l)\|_0 + \|D(l)\|_0. \quad (9)$$

In this prior, we take advantage of both BCP and DCP to facilitate the image deblurring problem. The effectiveness of the proposed ECP can be found in Section 5.1

4.2. Objective Function

We combine the proposed ECP based regularization term (9) into the recent single image deblurring framework in

[17], then our proposed objective function for image deblurring becomes

$$\begin{aligned} \{\hat{l}, \hat{k}\} = & \arg \min_{l, k} \|l \otimes k - b\|_2^2 + \gamma \|k\|_2^2 \\ & + \mu \|\nabla l\|_0 + \lambda \|D(l)\|_0 + \eta \|1 - B(l)\|_0, \end{aligned} \quad (10)$$

where $\gamma, \mu, \lambda, \eta$ are the corresponding weight parameters. The first term in Eq. (10) is the data fidelity term to restrict that the convolution of recovered image l should be consistent with the blurred image b . The difference between $l \otimes k$ and b are usually constrained by using the L_2 -norm [19, 26, 27] or the L_1 -norm [23, 18]. In this work, we use the L_2 -norm for the data fidelity function. The second term is a constraint which demands the blur kernel k to be stable. We adopt the L_2 -norm which can be solved by the Fast Fourier Transform (FFT) [19, 23]. The third term tends to retain the sharp image gradients but to remove tiny ones, while the fourth regularization term keeps the sparsity of the dark channels.

4.3. Optimization

Since it is difficult to obtain the solution of Eq. (10) directly, we instead use an alternating minimization algorithm based on the half-quadratic splitting algorithm [24]. The intermediate latent image l and the blur kernel k are estimated alternatively by fixing one of them, *i.e.*, the optimization problem becomes two sub-problems:

$$\begin{aligned} \hat{l} = & \arg \min_l \|l \otimes k - b\|_2^2 + \mu \|\nabla l\|_0 \\ & + \lambda \|D(l)\|_0 + \eta \|1 - B(l)\|_0, \end{aligned} \quad (11)$$

and

$$\hat{k} = \arg \min_k \|l \otimes k - b\|_2^2 + \gamma \|k\|_2^2. \quad (12)$$

We further present an efficient optimization algorithm to solve them accordingly.

4.3.1 Estimating Latent Image

Considering that the L_0 regularization term is computationally intractable, we propose an efficient algorithm to solve in Eq. (11) based on the half-quadratic splitting technique [24]. By introducing new auxiliary variables p, q and g , where $g = (g_h, g_v)^\top$, corresponding to $D(l)$, $1 - B(l)$ and ∇l , respectively, we can rewrite the objective function (11) as,

$$\begin{aligned} \{\hat{l}, \hat{g}, \hat{p}, \hat{q}\} = & \arg \min_{l, g, p, q} \|l \otimes k - b\|_2^2 + \alpha \|\nabla l - g\|_2^2 \\ & + \beta \|D(l) - p\|_2^2 + \omega \|1 - B(l) - q\|_2^2 \\ & + \mu \|g\|_0 + \lambda \|p\|_0 + \eta \|q\|_0, \end{aligned} \quad (13)$$

where α, λ and η are positive penalty parameters. The above optimization problem can be solved by alternatively

Algorithm 1 Our Deblurring Algorithm

Input: Blurry image b .
 generate the initial kernel k .
for $i=1:5$ **do**
 $l \leftarrow b, \omega \leftarrow 2\eta.$
repeat
 Solve for q using (20).
 $\beta \leftarrow 2\lambda.$
repeat
 Solve for p using (19).
 $\alpha \leftarrow 2\mu.$
repeat
 Solve for g using (18).
 Solve for l using (16).
 $\alpha \leftarrow 2\alpha.$
until $\alpha > \alpha_{\max}$.
 $\beta \leftarrow 2\beta.$
until $\beta > \beta_{\max}$.
 $\omega \leftarrow 2\omega.$
until $\omega > \omega_{\max}$.
 solve blur kernel k using (22)
 $\mu \leftarrow 0.9\mu, \lambda \leftarrow 0.9\lambda, \eta \leftarrow 0.9\eta.$
end for
Output: Intermediate latent image l and blur kernel k .

minimizing l , p , q and g separately while fixing the other variables. To solve the latent image l , the objective function becomes,

$$\hat{l} = \arg \min_l \|l \otimes k - b\|_2^2 + \alpha \|\nabla l - g\|_2^2 + \beta \|D(l) - p\|_2^2 + \omega \|1 - B(l) - q\|_2^2. \quad (14)$$

For the convenience of optimization, we reform our $1 - B(l)$ into $D(1 - l)$ for consistency. Note that the operation $D(l)$ is non-linear, similar to [17], we replace it with an equivalent linear operator M . The M is fundamentally a mapping matrix, which maps the pixel to its dark channel and is defined as,

$$M(x, y) = \begin{cases} 1, & y = \arg \min_{y \in \Omega(x)} l(y), \\ 0, & \text{otherwise.} \end{cases} \quad (15)$$

During the deblurring process, we use the intermediate latent image for computing M . When the intermediate image approaches the clear image, the computed M becomes closer to the operation D . Given the intermediate latent image l , we compute two mapping matrices M_l and M_{1-l} corresponding to $D(l)$ and $1 - B(l)$. Then, the objective function becomes,

$$\hat{l} = \arg \min_l \|l \otimes k - b\|_2^2 + \alpha \|\nabla l - g\|_2^2 + \beta \|M_l l - p\|_2^2 + \omega \|M_{1-l}(1 - l) - q\|_2^2, \quad (16)$$

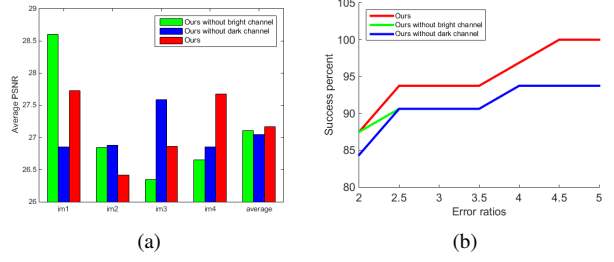


Figure 4. Quantitative evaluations on the benchmark dataset by [13] with and without using DCP or BCP. (a) Comparisons in terms of PSNR. (b) Comparisons in terms of cumulative error ratio.

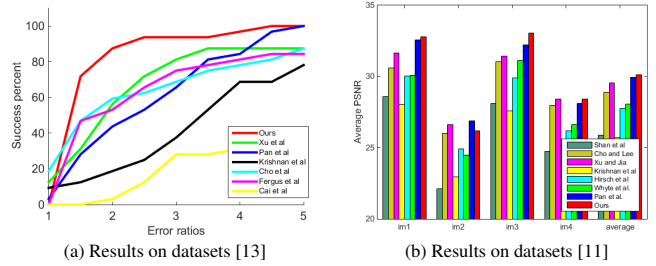


Figure 5. Quantitative evaluations on the benchmark datasets by [13] and [11], respectively.

in which l can be solved efficiently using the FFT,

$$\hat{l} = \mathcal{F}^{-1} \left(\frac{\overline{\mathcal{F}(k)\mathcal{F}(b)} + \alpha \mathcal{F}_g + \beta \mathcal{F}(p) + \omega \mathcal{F}(q)}{\overline{\mathcal{F}(k)\mathcal{F}(k)} + \alpha \overline{\mathcal{F}(\nabla)} \mathcal{F}(\nabla) + \beta + \omega} \right), \quad (17)$$

where $\mathcal{F}_g = \overline{\mathcal{F}(\nabla_h)} \mathcal{F}(g_h) + \overline{\mathcal{F}(\nabla_v)} \mathcal{F}(g_v)$; ∇_h and ∇_v denote the horizontal and vertical differential operators, respectively; $\mathcal{F}(\cdot)$ and $\mathcal{F}^{-1}(\cdot)$ denote the FFT and inverse FFT, respectively; and $\bar{\cdot}$ is the complex conjugate operator.

Given l , the subproblems with respect to g , p and q can be solved separately by:

$$\hat{g} = \arg \min_g \|\nabla l - g\|_2^2 + \mu \|g\|_0, \quad (18)$$

$$\hat{p} = \arg \min_p \beta \|D(l) - p\|_2^2 + \lambda \|p\|_0, \quad (19)$$

and

$$\hat{q} = \arg \min_q \omega \|1 - B(l) - q\|_2^2 + \eta \|q\|_0. \quad (20)$$

Note that Eq. (18) is a pixel-wise minimization problem, we obtain the solution of g according to [25]:

$$q = \begin{cases} 1 - B(l), & |1 - B(l)|^2 \geq \frac{\eta}{\omega}, \\ 0, & \text{otherwise,} \end{cases} \quad (21)$$

as well as solutions of p and q .



Figure 6. Comparisons of state-of-the-art methods on one challenging image from the dataset [11]. The deblurred image generated by the proposed algorithm with the bright channel prior is visually more pleasing.

4.3.2 Estimating Blur Kernel

In this subproblem, we optimize the blur kernel \hat{k} with the given l by employing the fast deblurring method [19] on the gradient images and the L_2 -norm of data fidelity term as:

$$\hat{k} = \arg \min_k \|\nabla l \otimes k - \nabla b\|_2^2 + \gamma \|k\|_2^2, \quad (22)$$

which is a least squares minimization problem. Similar to the existing approaches [19, 25], we compute the solution by FFT,

$$\hat{k} = \mathcal{F}^{-1} \left(\frac{\overline{\mathcal{F}(\nabla l)} \mathcal{F}(\nabla b)}{\overline{\mathcal{F} \nabla l} \mathcal{F}(\nabla l) + \gamma} \right). \quad (23)$$

In practice, we adopt a multi-scale blind deconvolution method for kernel estimation. In addition, we set the negative elements of k to zero and normalize k in the end. The main steps of our deblurring method are shown in the Algorithm 1.

5. Experimental Results

In this section, we analyze how our proposed algorithm performs on both the synthesized and real images and compare it to the state-of-the-art deblurring methods. In all experiments, the following fixed parameters are employed: $\mu = \lambda = \eta = 0.004$, $\gamma = 2$ and $\omega_l = 35$, where ω_l denotes the size of extreme channels patch. The Peak-Signal-to-Noise Ratios (PSNR) and the cumulative error ratio are used as the performance evaluation standards on kernel estimations and deblurred results.

5.1. Effectiveness of ECP

As mentioned in Sections 3 and 4, the proposed ECP regularization term considers more information in real situations. To demonstrate the effectiveness of the proposed ECP term, we compare the proposed method with the recent the DCP based image deblurring method [17] in image deblurring. We note that our method can naturally degrade to DCP based method [17] without the BCP in Eq. 8, and to only BCP based method without the DCP regularization term. We compare these three (BCP, DCP and ECP-based) methods on the dataset by [13], which is generated from 4 clear images and 8 different blur kernels. Figure 4(a) shows the quantitative evaluation of the proposed ECP based method against the DCP based method [17] and the BCP based approach in terms of PSNR. The proposed ECP based algorithm generates results with higher PSNR values than other two methods only condisering DCP or BCP.

In addition, we also show the performances of the proposed algorithm against the DCP-based [17] and BCP-based methods on this benchmark dataset [13] in terms of the cumulative error ratio. Figure 4(b) shows that the proposed ECP-based algorithm performs well on this dataset against the state-of-the-art DCP-based deblurring methods [17] in terms of cumulative error ratio, especially when the value is larger than 2 (which is close to real-world scenarios). Note that the BCP-based method also performs favorably against the state-of-the-art method [17] even without the DCP regularization, which further demonstrates the effectiveness of the proposed BCP and ECP-based methods.

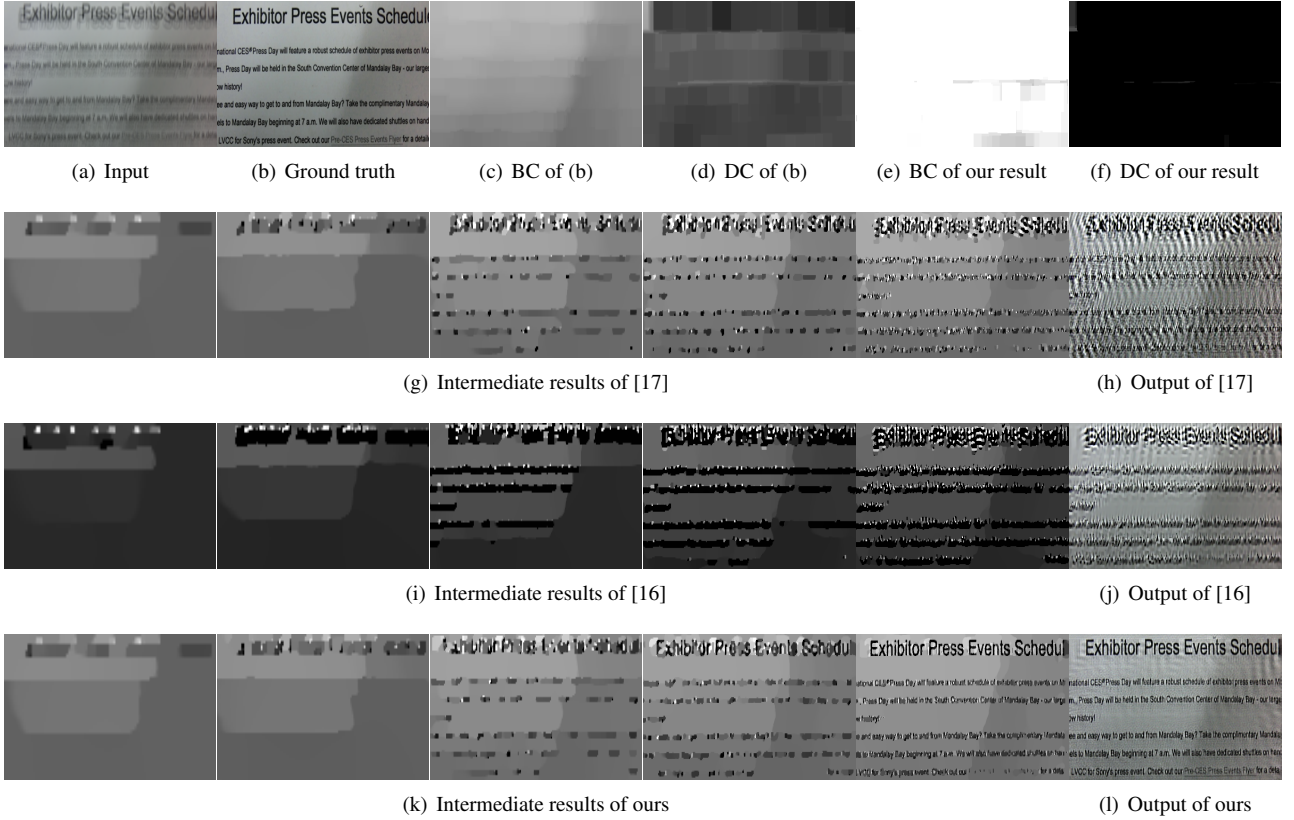


Figure 7. Comparisons with the state-of-the-art methods [16, 17]. (a) and (b) are the blurry input and corresponding ground truth image. (c) and (d) are the BC and DC of the image in (b). (e) and (f) are the BC and DC of the deblurred result by our method in (l). (g), (i) and (k) are the intermediate results over iterations (from left to right) by [17], [16] and our method, respectively. (h), (j) and (l) are the deblurred results by [17], [16] and our method, respectively. With the BCP and DCP, our method recovers intermediate results containing more sharp edges for kernel estimation. The dark channels of the intermediate results become darker and the bright channels become brighter, which favor clear images and facilitate kernel estimation.



Figure 8. Visual comparison of state-of-the-art methods on a real-world blurry image.

5.2. Synthetic Datasets

To better verify the effectiveness of our proposed method, we use the image benchmark datasets [13, 11] for quantitative evaluations and follow the protocols of [13, 11] for fair comparisons. We evaluate the performance of the proposed approach against the state-of-the-art methods

[13, 2, 5, 19, 12, 16, 25]. We first test on the dataset by Levin *et al.* [13]. Figure 5(a) indicates that our ECP based algorithm performs well against the state-of-the-art methods [2, 5, 19, 12, 16, 25] on this benchmark dataset [13] in terms of cumulative error ratio.

In addition, we also test the competing methods [20, 19, 23, 12, 7, 22, 17] on the benchmark dataset by [11], which includes 4 images and 12 blur kernels. We adopt the highest PSNR of those calculated by comparing the deblurred image with 199 ground truth images captured along the camera motion trajectory. Figure 5(b) contains quantitative evaluations in terms of the highest PSNR. Since the proposed method consider both BCP and DCP information, the PSNR values of the restored images by our method are higher than the state-of-the-art algorithms [20, 19, 23, 12, 7, 22, 17]. We further give a visual comparison in Figure 6, where the state-of-the-art methods do not generate clear images. While the method by Pan *et al.* [17] performs well against other approaches [20, 19, 23, 12, 22, 17], the generated im-

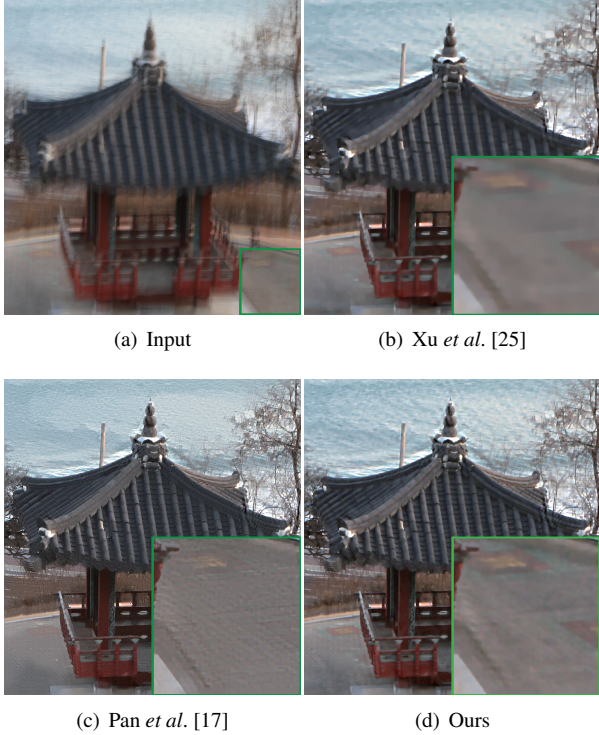


Figure 9. Visual comparison of state-of-the-art methods on a real-world blurry image.

age still contains significant ringing artifacts in the bottom of Figure 6(h). It is mainly because the large blur kernel blends the below dark part with some bright pixels, which makes DCP less effective. However, our method generates a clear image with fine textures as shown in Figure 6(j). Note that our method can generate visually pleasing image in Figure 6(i) even only using BCP based approach. The main reason is that the property of bright channel helps to remove the ring artifacts if there exist some bright regions in the input image.

In [17], dark channel also helps the blind deblurring on text images. We further carry out experiments on text images to demonstrate the effectiveness of the proposed BCP. Figure 7 visually shows our method performs well on a challenging blurry image against [17] and the method designed for text images [16]. As shown in Figure 7(g), (i) and (k), utilizing both the BCP and DCP generates clearer intermediate results. Meanwhile, our deblurred result in Figure 7(l) has less ringing artifacts compared to results generated by other methods [17, 16]. Note that the bright channel becomes extremely bright after the deblurring process, which demonstrates that our proposed L_0 -norm based on the BCP is helpful for kernel estimation and image deblurring. In particular, clear text images contain more bright pixels, which drives our BCP performing well.

5.3. Real Images

In this section, we test our method on real images against the recent state-of-the-art blind single image deblurring methods [25, 17]. We analyze the deblurring results qualitatively due to the unknown blur kernels and ground truth images. Figures 8 and 9 show two challenging real captured blurry images. The deblurred images generated by the proposed algorithm are sharper and clearer than others generated by [25, 17]. As shown in Figure 8, the face of the woman contains fewer edges or textures, which causes trouble for deblurring with the methods designed for natural images. Pan *et al.* [17] exploits the dark channel and performs well. However, the deblurred face still remains visually blurry artifacts. In contrast, by further utilizing our bright channel, our output becomes clearer in the face areas. Figure 9 demonstrates the results from an outdoor image. Comparing with other methods, our algorithm tends to recover sharper and clearer details as shown in Figure 9(d).

6. Conclusion

In this paper, we propose a novel BCP based on the observation that these bright pixels in the clear images will become less bright after the blurring process. By combining this prior with DCP, we propose an effective prior, named ECP, to recover the latent images for kernel estimation. The proposed method considers both the dark and bright channels information and does not require any complex processing techniques or edge selection steps. Extensive experimental results on both the synthesized and natural images demonstrate that the proposed algorithm performs favorably against the state-of-the-art deblurring methods. In addition, we believe that our proposed prior can motivate further research and the development of novel applications in a variety of fields.

Acknowledgements: Supported by National Key Research and Development Plan (No.2016YFB0800403),National Natural Science Foundation of China (No.61422213, U1636214), Beijing Natural Science Foundation4172068,Key Program of the Chinese Academy of Sciences (No. QYZDB-SSW-JSC003).

References

- [1] P. Arbelaez, J. Pont-Tuset, J. T. Barron, F. Marques, and J. Malik. Multiscale combinatorial grouping. *In CVPR*, 2014.
- [2] J.-F. Cai, H. Ji, C. Liu, and Z. Shen. Framelet-based blind motion deblurring from a single image. *IEEE TIP*, 21(2):562–572, 2012.
- [3] X. Cao, W. Ren, W. Zuo, X. Guo, and H. Foroosh. Scene text deblurring using text-specific multiscale dictionaries. *IEEE TIP*, 24(4):3426–3437, 2015.

- [4] T. Chan and C. Wong. Total variation blind deconvolution. *IEEE TIP*, 7(3):370–375, 1998.
- [5] R. Fergus, B. Singh, A. Hertzmann, S. T. Roweis, and W. T. Freeman. Removing camera shake from a single photograph. *ACM Transactions on Graphics*, 25(3):787–794, 2006.
- [6] K. He, J. Sun, and X. Tang. Single image haze removal using dark channel prior. *In CVPR*, 2009.
- [7] M. Hirsch, C. J. Schuler, S. Harmeling, and B. Schlkopf. Fast removal of non-uniform camera shake. *In ICCV*, 2011.
- [8] Z. Hu, S. Cho, J. Wang, and M.-H. Yang. Deblurring low-light images with light streaks. *In CVPR*, 2014.
- [9] Z. Hu, L. Yuan, S. Lin, and M.-H. Yang. Image deblurring using smartphone inertial sensors. *In CVPR*, 2016.
- [10] N. Joshi, R. Szeliski, and D. J. Kriegman. Psf estimation using sharp edge prediction. *In CVPR*, 2008.
- [11] R. Kohler, M. Hirsch, B. J. Mohler, B. Scholkopf, and S. Harmeling. Recording and playback of shake: Benchmarking blind deconvolution with a real-world database. *In ECCV*, 2012.
- [12] D. Krishnan, T. Tay, and R. Fergus. Blind deconvolution using a normalized sparsity measure. *In CVPR*, 2011.
- [13] A. Levin, Y. Weiss, F. Durand, and W. T. Freeman. Understanding and evaluating blind deconvolution algorithms. *In CVPR*, 2009.
- [14] A. Levin, Y. Weiss, F. Durand, and W. T. Freeman. Efficient marginal likelihood optimization in blind deconvolution. *In CVPR*, 2011.
- [15] T. Michaeli and M. Irani. Blind deblurring using internal patch recurrence. *In ECCV*, 2014.
- [16] J. Pan, Z. Hu, Z. Su, and M.-H. Yang. L0-regularized intensity and gradient prior for deblurring text images and beyond. *IEEE TPAMI*, 2016.
- [17] J. Pan, D. Sun, H. Pfister, and M.-H. Yang. Blind image deblurring using dark channel prior. *In CVPR*, 2016.
- [18] W. Ren, X. Cao, J. Pan, X. Guo, W. Zuo, , and M.-H. Yang. Image deblurring via enhanced low-rank prior. *IEEE TIP*, 25(7):3426–3437, 2016.
- [19] S.Cho and S.Lee. Fast motion deblurring. *ACM Transactions on Graphics*, 28(5):145, 2009.
- [20] Q. Shan, J. Jia, and A. Agarwala. High-quality motion deblurring from a single image. *ACM Transactions on Graphics*, 27(3):73, 2008.
- [21] L. Sun, S. Cho, J. Wang, and J. Hays. Edge-based blur kernel estimation using patch priors. *In ICCP*, 2013.
- [22] O. Whyte, J. Sivic, A. Zisserman, and J. Ponce. Non-uniform deblurring for shaken images. *In IJCV*, 98(2):168–186, 2012.
- [23] L. Xu and J. Jia. Two-phase kernel estimation for robust motion deblurring. *In ECCV*, 2010.
- [24] L. Xu, C. Lu, Y. Xu, and J. Jia. Image smoothing via l0 gradient minimization. *ACM Transactions on Graphics*, 30(6), 2011.
- [25] L. Xu, S. Zheng, and J. Jia. Unnatural l0 sparse representation for natural image deblurring. *In CVPR*, 2013.
- [26] L. Zhong, S. Cho, D. Metaxas, S. Paris, and J. Wang. Handling noise in single image deblurring using directional filters. *In CVPR*, 2013.
- [27] Y. Zhou and N. Komodakis. A map-estimation framework for blind deblurring using high-level edge priors. *In ECCV*, 2014.